Supplemental material

Sallé et al., https://doi.org/10.1083/jcb.201807102

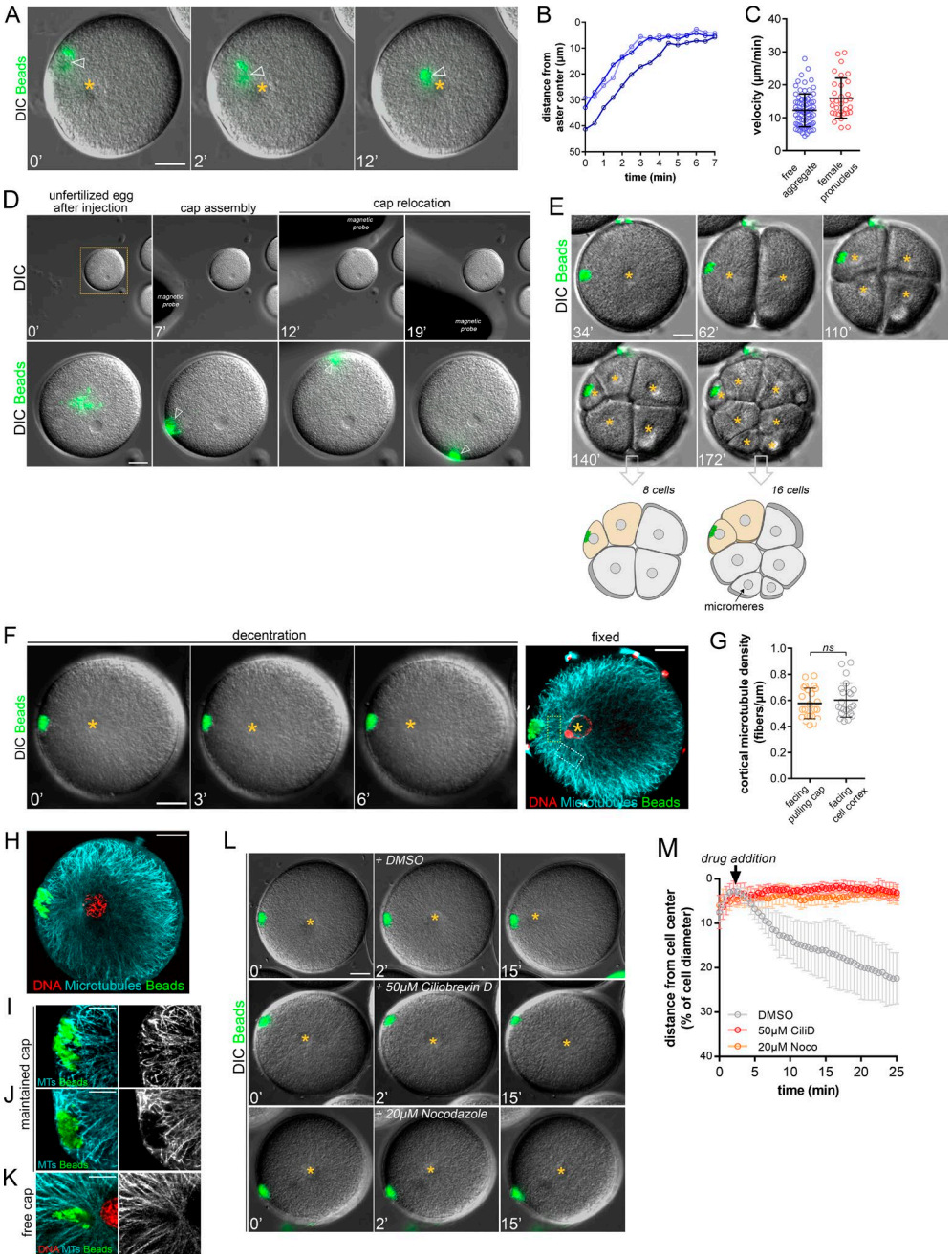

Figure S1. **Cortical pulling from magnetic beads domains depends on MTs and dynein.** Related to Fig. 1. **(A)** Time-lapse sequence showing the centripetal motion of a free aggregate during aster centration. Orange star: the aster center; arrowhead: the position of the aggregate. Bar, 20 µm. **(B)** Quantification of the distance between a free cap and aster center during centration. Three representative cases are displayed. **(C)** Quantification of free aggregate and female pronucleus velocity during aster centration (n = 78 and n = 33, respectively). Error bars correspond to SDs. **(D)** Time-lapse sequence showing cortical cap assembly and relocation in an unfertilized egg. Top: Low-magnification view of the egg and the different magnetic probe positions. Bottom: Details of cap assembly and relocation around the same cell (arrowhead). **(E)** Time-lapse sequence of small cap maintained during subsequent embryonic divisions. Note how the cap can drive asymmetric division in the small four-cell blastomere but not in bigger one- and two-cell-stage blastomeres. 8 and 16 cell stages are schematized to illustrate the cap-induced asymmetric divisions (yellow blastomeres) that occur independently of endogenous micromere generation. **(F)** Time-lapse sequence of a decentering aster under cortical pulling. Yellow star: aster center/zygote nucleus. Right: Confocal image of the same embryo after in situ fixation. Red: DNA; cyan: MTs; green: beads. Bars, 20 µm. **(G)** Quantification of MT density during aster decentration in the region facing the pulling cap (orange dotted box in F) and in the region facing the cell cortex (white dotted box in F; n = 23). Error bars correspond to SD. **(H)** Confocal image of a decentered aster in late interphase. Colors as in F. Bars, 20 µm. **(I–K)** Details of the MTs network surrounding a maintained pulling cap (I and J) and a free cap moving toward the aster center (K). Note that I corresponds to a magnification of the region surrounding the cap in H. Colors as in F. Bar, 10 µm. **(L and M)** Inhibition of MT and dynein prevent aster decentration from the cortical domain. The chemical inhibitors were added after centration. Top: Control DMSO; middle: 50 µM Ciliobrevin D (CiliD); bottom: 20 µM Nocodazole (Noco). **(M)** Quantification of the impact of chemical inhibitors on aster decentration by the domain. Error bars correspond to SD. Final aster positions were compared by using a two-tailed Mann–Whitney test. P = 0.0095 for CiliD and 0.0286 for Nocodazole.

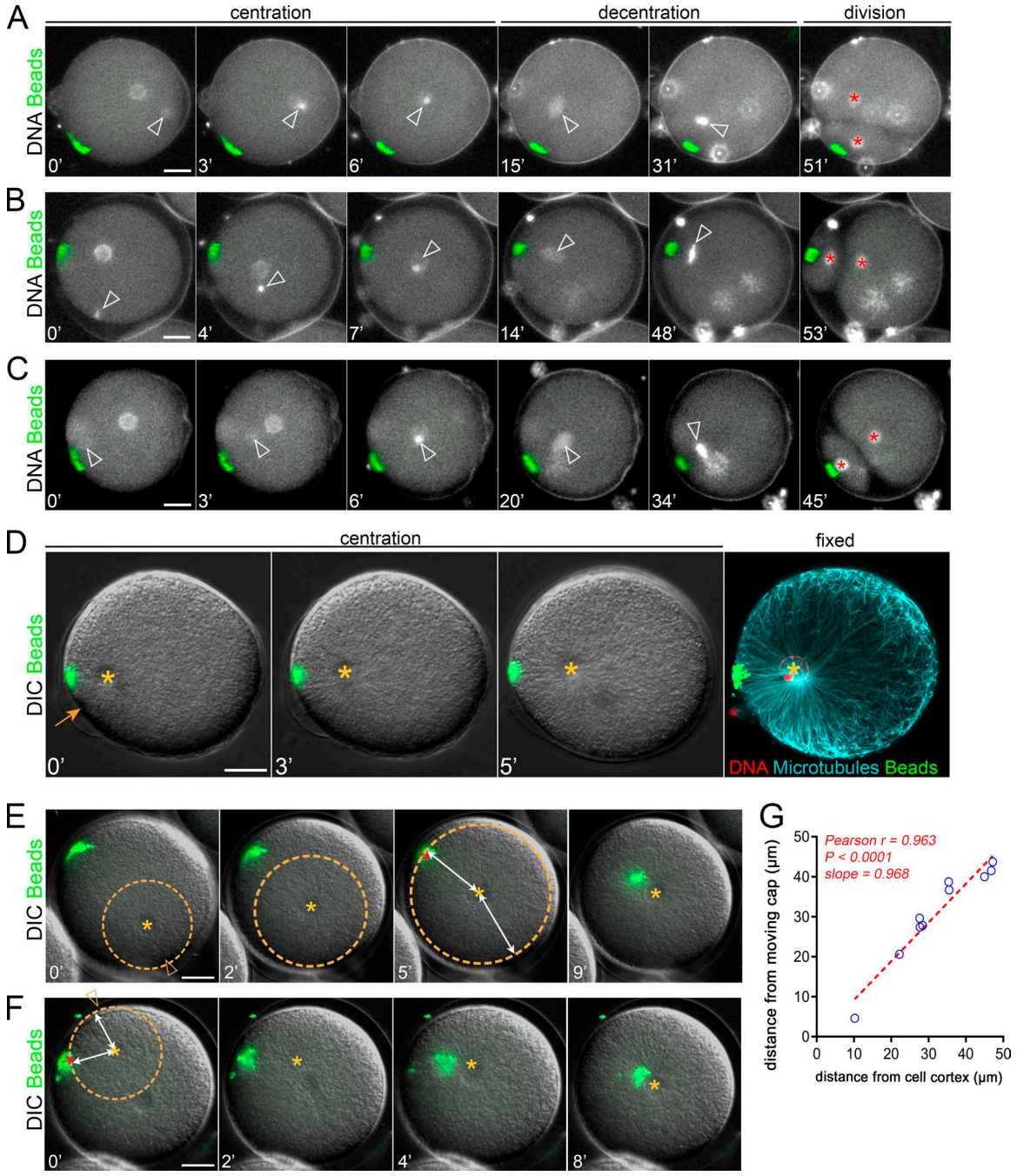

Figure S2. **Aster centration and decentration under cortical pulling. (A–C)** Time-lapse sequences showing successive aster centration and decentration under cortical pulling forces when fertilization occurs: at the opposite of the cap (A), ~90° relative to the cap (B), and close to the cap (C). Arrowheads: the position of the nuclei at the center of asters; red stars: the blastomere nuclei after division. Contrast is adjusted to compensate for an increase in DNA labeling (Hoechst). **(D)** Time-lapse sequence of a centering under cortical pulling. Arrow: the site of sperm entry; yellow star: aster center/zygote nucleus. Right: Confocal image of the same embryo after in situ fixation. Red: DNA; cyan: MTs; green: beads. Bars, 20 µm. **(E and F)** Time-lapse sequences illustrating the link between aster growth and the start of aggregate centripetal motion during late (E) and early (F) centration. Orange arrowheads: sperm entry point; orange circle and star: the estimated aster size and aster center, respectively. Red arrows: the beginning of aggregate centripetal motion. Bars, 20 µm. **(G)** Correlation between aster radius and the shortest distance at which free aggregates are attracted toward aster center (white arrows in E and F).

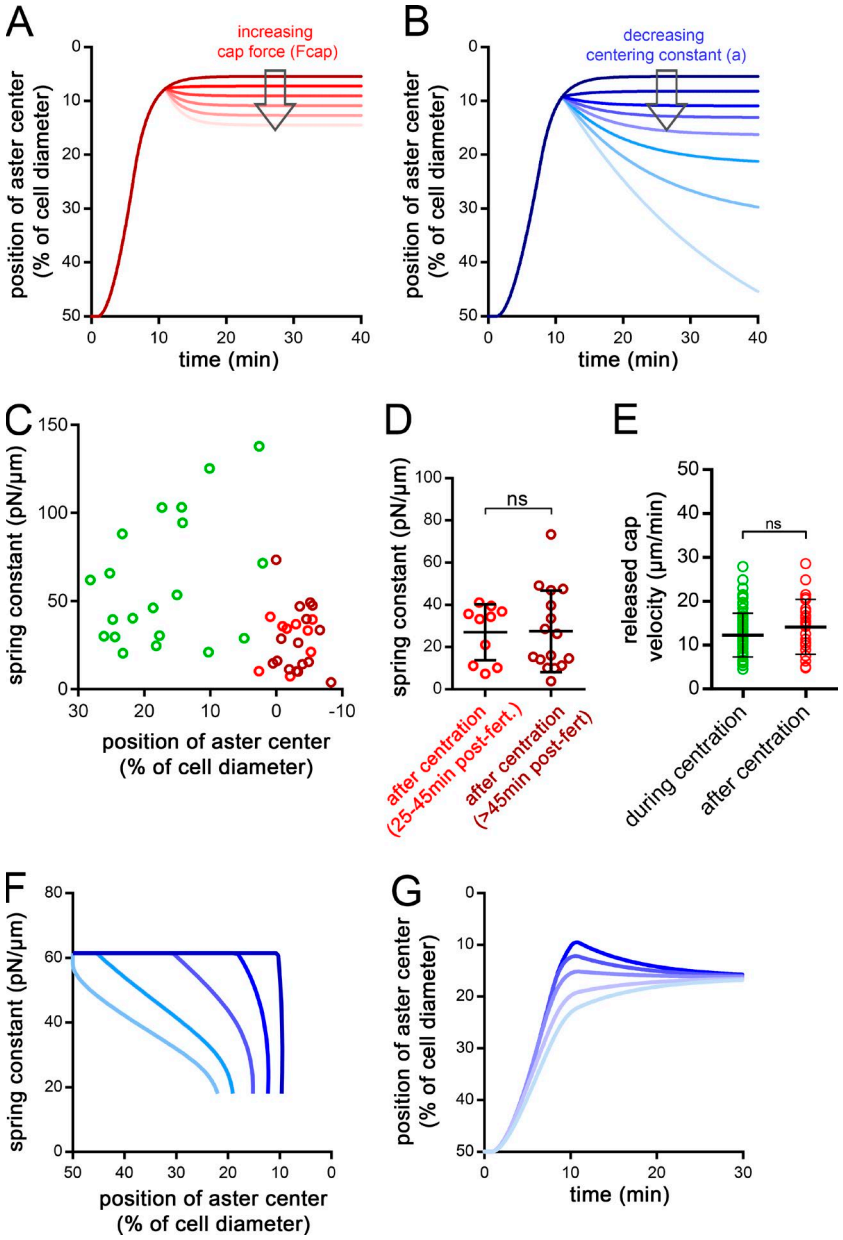

Figure S3. **Influence of aster centering stiffness dynamics on centration and decentration. (A and B)** Aster position dynamic in the 1D model when the cap pulling force, F_{cap}, is increased in a dose-dependent manner after centration (A) or when aster centering force coefficient, *a*, is decreased in a dose-dependent manner after centration (B). **(C)** Measured spring constants during centration (in green) and after centration (in red) plotted as a function of aster position relative to the cell center. Negative values on the x axis correspond to a slight overshoot in the centered position. **(D)** Average spring constant values measured early after centration (25–45 min after fertilization [post-fert], light red; *n* = 10) and late after centration (>45 min post-fert, dark red, *n* = 16). The same datasets are also displayed in C. **(E)** Quantification of the velocity of a released bead cap during and after centration (*n* = 78 and *n* = 24, respectively). In D and E, error bars correspond to SD, and results were compared by using the two-tailed Mann–Whitney test. ns, P > 0.05. **(F and G)** Effect of aster centering stiffness dynamics in 3D simulation. Different transition kinetics between centration and postcentration stiffness were tested (F) and their impact on aster trajectories assessed (G).

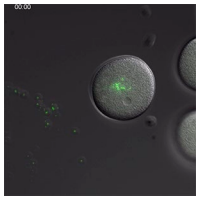

Video 1. **Pulling cap assembly and relocation.** Unfertilized egg after magnetic bead injection. Embryos were visualized using differential interference contrast; beads are in green. The magnetic probe is used to assemble and relocate a cortical pulling cap. Images were obtained by wide-field time-lapse microscopy. Frames were taken every 30 s for 17 min.

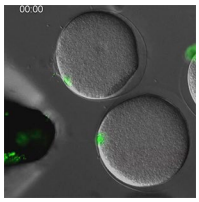

Video 2. **Asymmetric division induced by artificial cortical pulling.** A cortical pulling cap is maintained during the first cleavage in embryos by using a magnetic probe. Embryos were visualized using differential interference contrast; the beads forming the pulling cap are in green. Images were obtained by wide-field time-lapse microscopy. Frames were taken every 10 s for 98 min.

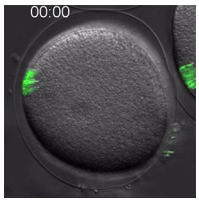

Video 3. **"Free cap" control embryo.** First cleavage visualized in an embryo containing a free pulling cap (no magnet). Embryos were visualized using differential interference contrast; the beads are in green. Images were obtained by wide-field time-lapse microscopy. Frames were taken every 20 s for 63 min.

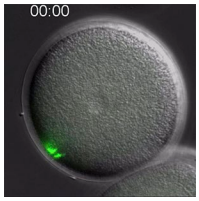

Video 4. **"Non-pulling cap" control embryo.** First cleavage visualized in an embryo containing a nonpulling cap maintained at the cortex. Embryos were visualized using differential interference contrast; the beads forming the cap are in green. Images were obtained by wide-field time-lapse microscopy. Frames were taken every 30 s for 62 min.

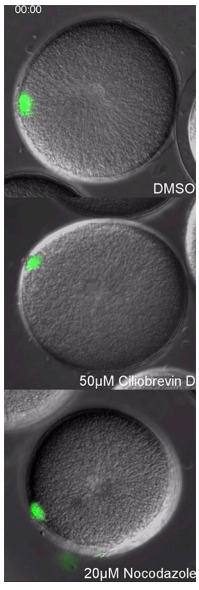

Video 5. **Decentration after dynein motors inhibition or MT depolymerization.** Nucleus decentration after drug addition (white square at the bottom left corner of each video). From top to bottom: DMSO; 50 µM Ciliobrevin D; 20 µM Nocodazole. Embryos were visualized using differential interference contrast; the beads forming the cap are in green. Images were obtained by wide-field time-lapse microscopy. Frames were taken every 30 s for 15 min.

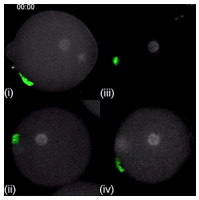

Video 6. **Aster centration and decentration under cortical pulling.** Aster center was visualized using male pronucleus and zygote nucleus DNA (after pronuclei fusion) in white. Beads forming the pulling cap are in green. The four panels represent different angles between the pulling cap and the sperm entry point: (i) ∼120°, (ii) ∼80°, (iii) ∼40°, and (iv) ∼5°. Images were obtained by wide-field time-lapse microscopy. Frames were taken every 30 s for up to 61 min.

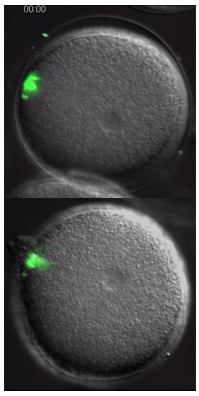

Video 7. **"Free cap" during centration.** Centration was visualized using differential interference contrast, and beads forming the free pulling cap (no magnet) are in green. In the top video, fertilization occurs close to the cap, while in the bottom video, fertilization occurs on the opposite cortex. Images were obtained by wide-field time-lapse microscopy. Frames were taken every 30 s for 20 min.

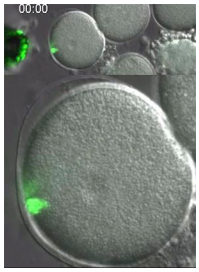

Video 8. **Magnetic force reduction during aster centration under cortical pulling.** Centration was visualized using differential interference contrast; beads forming the pulling cap are in green. Top: An embryo containing a pulling cap moving away from the magnetic probe. Bottom: A registered and magnified view of the same embryo. Images were obtained by wide-field time-lapse microscopy. Frames were taken every 30 s for 14 min.

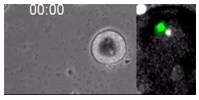

Video 9. **Aster pulling during and after centration.** Two short magnetic pulls were applied, perpendicular to the centration axis (horizontal) during and after centration. The left panel (differential interference contrast) shows a low-magnification view of the embryo and magnet. The right panel shows the same embryo containing a beads aggregate bound to the aster center. DNA is in white, and beads are in green. Images were obtained by wide-field time-lapse microscopy. Frames were taken every 20 s for 44 min.

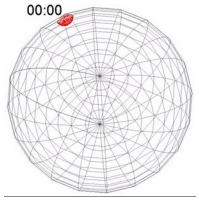

Video 10. **3D simulation of aster centration and decentration under cortical pulling.** MTs are in green, aster trajectory is in blue, and the pulling cap is represented as a red hemisphere. Frames were taken every 20 s for 50 min.